Laser micromachining of TiN coatings with variable pulse durations and shapes in ns regime

Ali Gökhan Demir [a,*], Krste Pangovski [b], William O'Neill [b], Barbara Previtali [a]

[a] Department of Mechanical Engineering, Politecnico di Milano, Via La Masa 1, 20156 Milan, Italy
[b] Institute for Manufacturing, University of Cambridge, 17 Charles Babbage Road, Cambridge CB3 0FS, United Kingdom

Received 8 November 2013
Accepted in revised form 10 September 2014
Available online 19 September 2014

1. Introduction

Ceramic surface coatings are extensively applied for various purposes, encompassing mechanical, biomedical, and electronic applications. Ceramic surface coatings applied as superficial layers are of interest for improving the performance of components because of their superior properties in terms of mechanical, thermal and chemical stability. In particular, TiN coatings are extensively used in industrial applications, such as cutting tools, dies and moulds, biomedical implants, and components used in food industries, as well as for decorative purposes [1–3]. Recently, the surface structuring and machining of these coatings have gained increasing attention. Because the coating layer is limited to a very small thickness (a few μm), the machining conditions required can be fulfilled by micro-processing techniques. The high hardness and fragile nature of ceramic coatings should also be considered during process selection. The traditional chip removal processes are not adaptable to surface structuring of ceramic coatings. Chemical etching processes are applicable, although the corrosion stability of the material can limit their feasibility. However, the direct writing of desired patterns with laser micromachining provides a flexible solution with high machining resolution, flexibility in machined geometries, and reduced lead times between design and production, because the process does not necessarily require dies or masks. The laser micromachining applications of TiN coatings include microdrilling for the enhanced fixation of dental implants [4], surface micromachining of sensors and actuators in MEMS [5], and surface texturing for the improved tribological performance of mechanical components [6], among others. In addition to surface patterning, laser micromachining has also been used to remove TiN layers from cutting tools [7].

The processing quality of the laser micromachining of ceramic coatings, as in the case of all laser ablation based process, mainly depends on the laser wavelength (λ) and pulse duration (τ). These two factors combined determine the interaction between the laser and matter. The laser wavelength is the principal parameter in determining the absorption of laser energy by the machined material, although absorption is a dynamic phenomenon that depends on time-dependant physical parameters, such as temperature. Thus, absorption is likely to vary even within the duration of a single laser pulse. Moreover, shorter wavelengths can provide higher machining resolution due to enhanced laser beam focusability. The pulse duration is generally categorised as long pulses (ms, μs), short pulses (ns), and ultrashort pulses (ps, fs). Ultrashort pulses provide better machining quality, because the interaction time between the material and the light is sufficiently short to prevent electron–lattice coupling [8]. The process depends on optical penetration, and the ablation conditions yield direct removal from solid. With increasing pulse duration, electron-lattice coupling is fulfilled, and the heat penetrates into the bulk material. Heat diffusion within the bulk material causes temperature gradients, which lead to the vaporisation or melting of different material fractions. Common defects in laser

* Corresponding author.
E-mail address: aligokhan.demir@polimi.it (A.G. Demir).

micromachining, namely, heat-affected zones, dross and recast, result from this effect. Although longer pulses are characterised by such defects, laser sources operating with longer pulses are widely used at the industrial scale with large pulse energies and high pulse repetition rates, which provide faster machining conditions.

The interactions between laser beams and TiN coatings have been investigated in the literature based on different combinations of wavelength and pulse duration. The effect of μs pulses generated with a CO_2 laser on TiN coatings demonstrated a melt dominant material removal mechanism [9–11], although the resulting machining quality was far from that required for high-precision micromachining. It was reported that ns pulses generated with KrCl ($\lambda = 222$ nm) [10] and XeCl ($\lambda = 308$ nm) [11] excimer lasers generated significantly smaller melt fractions generated in comparison to μs pulses. Kononenko et al. [12] compared the effect of ns and ps pulse durations using combinations of UV (270 nm), visible (539 nm), and IR (1078 nm) wavelengths. The authors reported no significant change in ablation rate as a function of wavelength used due to the constant optical penetration depth in the wavelengths employed. The same observation was presented for the pulse durations employed (150 ps–9 ns); however, the authors reported increased heat affected zones with ns pulses due to increased heat penetration depth. In another work, the micromachining of TiN with fs pulses was reported to yield melt free, vaporisation dominant ablation conditions with high machining quality [13].

Although wavelength and pulse duration are the major factors that determine micromachining quality, other parameters, such as the beam quality factor (M^2), transverse electromagnetic mode (TEM), and pulse-to-pulse energy stability, are of high importance for high-precision and robust micromachining operations. Pulse shape is one of the less explored parameters with respect to micromachining quality. For a preliminary distinction, pulse duration is adequate; however, to better comprehend the ablation phenomenon, pulse duration alone is not satisfactory. The same amount of energy can be delivered with the same pulse duration when delivered according to different temporal shapes. Because every material-laser beam couple constitutes different conditions, the usual conventions regarding the pulse duration, such as full-width at half-maximum (FWHM), or the pulse intensity, such as fluence and irradiance, can create ambiguities during comparison. The distinctions between the forms are more crucial under conditions in which the pulse duration is significantly higher than the lattice cooling temperature of the material (which is in the order of ps), for example, in the case of ns pulses. Changes in the nature of machining occur when using ns pulses due to fast ascending peaks; more specifically, Si can be machined with 1064 nm wavelength laser, to which the material is transparent at room temperature [14]. With the development of new generation of solid state lasers that possess pulse form and duration programmability, laser micromachining with ns pulses has attained increased flexibility during operation and a larger margin of quality improvement, which are critically important factors for industrial scale production.

The present work presents the characterisation of laser micromachining of TiN coatings on AISI M2 tool steel with a variety of pulse durations and shapes in the ns regime using a master oscillator pulse amplifier (MOPA) fibre laser. The pulse durations and shapes were selected and analysed within the 12–200 ns range. Single- and multiple-pulse ablation conditions were investigated to better comprehend the roles of the pulse components, including the duration, energy, and peak power. In particular, different ablation conditions within the ns regime were investigated in single-pulse ablation, where a quantitative analysis of the influence of pulse duration on ablation fluence and irradiance thresholds was attempted. In a large pulse duration range using singular intensity parameters, such as the threshold fluence or irradiance was observed to be inadequate, because inverse behaviour was observed as a function of pulse duration in these two parameters. Accordingly, the pulse shapes were decomposed to explain the role of the primary peak and tail. A regression model was fitted to better explain the ablation phenomenon using the decomposition parameters. Under multiple-pulse conditions, the percussion drilling of the coating was investigated as a function of the pulse shape and duration, energy and number of pulses emitted. The effects on hole geometry and quality were discussed. The results were interpreted both from a physical point of view to explain different machining conditions, as well as to indicate the preferential conditions for better quality and higher productivity.

2. Materials and methods

The substrate was quenched and tempered 12-mm-thick AISI M2 tool steel with a ground surface finish. The TiN coating was deposited by cathodic arc physical vapour deposition (Lafer SpA, Piacenza, Italy). The coating was deposited at 450 °C for a total duration of 1 h 45 min. This substrate was matched to the coating, because the combination suitably represents coated deformation and cutting tools. The measured coating thickness was estimated as 3.91 ± 0.09 μm, whereas the average coating roughness was $R_a = 0.80 \pm 0.06$ μm perpendicular to the grinding direction. The physical properties of the coating and substrate materials are listed in Table 1. An active fibre laser with a master oscillator pulse amplifier (MOPA) architecture and pulse-tuning capability was employed for the study (SPI G3 20P-HS, Southampton, UK). The laser source was programmable to produce different durations varying between 9 ns and 200 ns, with a maximum pulse energy of 0.8 mJ available for the longest pulse duration. Beam positioning was achieved via a scanner head (Nutfield XLR8-15-1064, Hudson, NH, USA), which housed a 125-mm focal lens. The system specifications are detailed in Table 2.

The pulses generated with the present laser source were characterised by fast ascending peaks and tails that decayed at relatively slower rates. Decreasing the pulse duration did not change the primary peak but shortened the decay tail. For this study, pulse durations of 12 ns, 30 ns, 65 ns, 100 ns, 150 ns, and 200 ns were chosen. Fig. 1 depicts the pulse shapes of the chosen pulse durations with and similar peak powers. Bell-shaped symmetry around the peak power value is present only with shorter pulses of 12 ns and 30 ns. Hence, for a given pulse duration, the pulse energy variation changes the pulse shape for longer pulses. Between 65 and 200 ns, the pulse peak shape flattens as the energy is reduced; in contrast, with 12 ns and 30 ns pulses, the symmetry is maintained.

The experimental work consisted of two phases. In the initial phase, the single-pulse ablation of TiN coatings was investigated as a function of fluence (F[J/cm^2]), irradiance (I[MW/cm^2]), and pulse duration (τ[ns]), with the first two defined as:

$$F = 2E_p/\left(\pi {w_s}^2\right) \tag{1}$$

$$I = 2P_{peak}/\left(\pi {w_s}^2\right) \tag{2}$$

where E_p is the pulse energy, P_{peak} is the pulse peak power, and w_s is the laser spot radius at the material surface. All experiments were carried out with the focal plane on the surface, thus the laser spot radius, w_s, was equal to the radius at the focal plane ($w_s = w_0$), calculated as:

$$w_0 = \lambda M^2 f/(\pi w_c) \tag{3}$$

Table 1
The physical properties of the coating and substrate material [15–19].

Property		TiN	AISI M2
Density	ρ (kg/m^3)	5220	8160
Melting temperature	T_m (K)	3223	1723
Heat capacity	c_p (J/kgK)	702.6	500
Thermal conductivity	K (W/mK)	19.2	21.3
Thermal diffusivity	α (m^2/s)	5.24e−6	5.22e−6
Reflectivity at 1064 nm	R	80%	65% (Fe)

Table 2
The details of the laser micromachining system.

SPI G3 20P-HS	
Max. average power	20 W
Pulse repetition rate	1–500 kHz
Emission wavelength	1064 nm
Maximum pulse energy	0.8 mJ
Beam quality factor M^2	≤2
Output beam diameter	3.1 mm
Beam expansion	×3
Focal lens	125 mm
Beam radius at focal plane	18.2 μm

where λ is the laser wavelength, M^2 is the beam quality factor, f is the focal length of the focusing lens, and w_c is the collimated beam radius projected on the focusing lens [16].

The ablated area diameter was measured from optical microscopy images (Olympus BX51, Melville, NY, USA). SEM (Zeiss EVO-50, Oberkochen, Germany) images were collected in secondary electron and back scattered emission modes. Morphological analysis was carried out on the SEM images to reveal the effect of peak power, energy, and pulse duration on the ablation mechanisms and quality. The effect of pulse duration was compared between machining conditions, characterised by similar energy and similar peak power levels.

To quantify the effects of the pulse energy and peak power separately, the threshold fluence and irradiance values were calculated for different pulse durations. The threshold fluence and irradiance were calculated according to the model proposed by Liu [20]. The threshold fluence was calculated as:

$$D^2 = 2{w_0}^2 \ln(F/F_{th}) \tag{4}$$

while the threshold irradiance was calculated as:

$$D^2 = 2{w_0}^2 \ln(I/I_{th}) \tag{5}$$

where D is the ablated zone diameter, and F_{th} and I_{th} are the ablation threshold fluence and irradiance, respectively. Thus far, the model proves to be adaptable to shorter *ps*, and *fs* pulses, which provide thermal effect-free ablation conditions, thus free of melt generation. Therefore, the measured area reflects the effective beam size capable of ablating the material surface. Provided that the ablated region is free of melt and can be easily defined, the model can also be applied to longer pulse durations. The model assumes a Gaussian energy distribution of the laser beam. Although the laser sources used in this work had a beam quality factor of $M^2 \leq 2$, the beam shape was characterised by a single sharp peak at the centre, suitable for being estimated as a near-Gaussian beam [14]. The ablation threshold fluence and irradiation were calculated using a nonlinear regression method by means of statistical software (Minitab). The method uses an iterative algorithm (Gauss–Newton) to match the unknowns of the non-linear regression equation starting from set values and then diverges to the best fit. The known parameters of the non-linear regression are the measured ablated area diameters, D, and the pulse energy, E_p, in the case of threshold fluence (P_{peak} in the case of threshold irradiance). The unknowns that are estimated through the algorithm are the beam radius at the focal position, w_0, and the ablation threshold fluence, F_{th} (or threshold irradiance I_{th}). It is preferable to set both w_0 and F_{th} (or I_{th}) as the unknowns of the equation, because slight variations of the spot radius are expected during experimentation. In this case, the advantage is that the statistical confidence intervals for the mean are calculated to the equation unknowns, providing a direct value of the error developed during the calculation of the threshold fluence and irradiation values. The forms of the equations with the two unknowns as used here are given below:

$$D^2 = 2w_0^2 \ln\left(\frac{2E_p / w_0^2\pi}{F_{th}}\right) \tag{6}$$

$$D^2 = 2w_0^2 \ln\left(\frac{2P_{peak} / w_0^2\pi}{I_{th}}\right). \tag{7}$$

The ablation threshold model has been widely used since its introduction. It is an effective model for distinguishing the ablation characteristics of different materials for fixed pulse durations. However, over large ranges in pulse durations, especially when ns pulses are concerned, the model can generate ambiguities. Due to thermal interaction, the pulse shape becomes critically important, because it determines the rate of energy deposition to the material. To introduce the various effects of pulse energy and peak power into a single model, a pulse decomposition approach was introduced. A statistical regression model was fitted over the experimental data to quantify the effects of the separate pulse components.

In the second phase of the experimental work, a multiple-pulse study was performed. The number of pulse durations used was reduced to three values, namely, 12 ns, 100 ns, and 200 ns. The pulse number was varied to drill into the coating and then into the substrate, to reveal the effect of changes in material response when switching from the coating material to the substrate. Optical microscopy and SEM images were collected to investigate the machining behaviour and measure the diameter of the hole drilled. A white light interferometer system (Veeco NT3300, Plainview, NY, USA) was used to measure the depth (h) of each hole, defined as the distance of the lowest point of the realised crater from the material surface. The hole depth was also taken as an indicator of the layer machined. The parameter sets for the two experimental phases are summarised in Table 3.

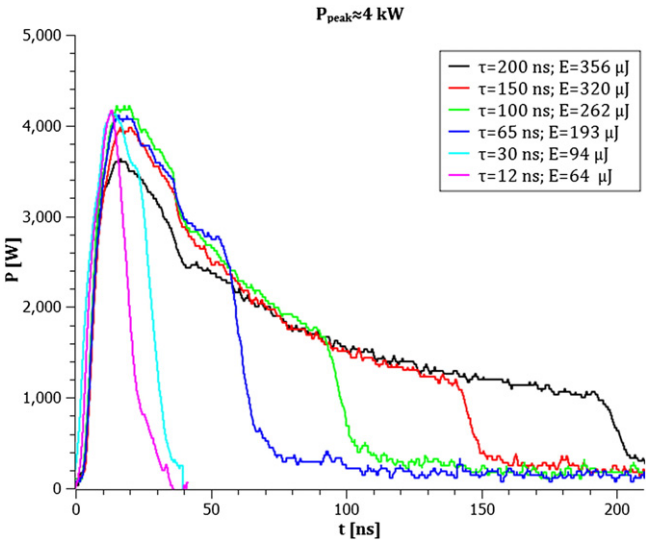

Fig. 1. The shape characteristics of the different pulse durations.

3. Results and discussion

3.1. Single-pulse study

Fig. 2 presents the ablation conditions of different pulse durations with an average pulse energy of 76.8 μJ. Injecting the same amount of energy in longer pulse durations decreases the size of the ablated zone. Although the process is dominated by vaporisation, slight melt formation is visible around the edges for longer pulses of 100 ns,

Table 3
The parameter sets of the single and multiple pulse studies.

Single pulse study						
Pulse duration	12 ns	30 ns	65 ns	100 ns	150 ns	200 ns
Pulse energy	5–77 μJ	7–114 μJ	13–193 μJ	19–262 μJ	31–320 μJ	72–356 μJ
Focal position	0 mm					
Multiple pulse study						
Pulse duration		12 ns		100 ns		200 ns
Pulse energy		9–36 μJ		19–262 μJ		72–356 μJ
Number of pulses		9–81		3–14		3–9
Focal position		0 mm				
Pulse repetition rate		20 kHz				

150 ns, and 200 ns. However, there is no evidence for the formation of spatter or melt droplets around the ablated zones. Cracks are visible inside the ablated zones, although they tend to become less prominent with shorter pulses, indicating that the thermal affect decreases with reduced pulse duration (see the insets in Fig. 2). Fig. 3 presents the ablation conditions with different pulse durations and an average pulse peak power of 3 kW. It can be observed that the ablated area is enlarged with longer pulse durations. However, the previous observations in terms of melt generation and crack size inside the ablated zones also remain valid in this case. In the processing conditions reported in Figs. 2 and 3, the ablation conditions yielded very limited material removal. The TiN coating was incompletely removed, because the ablation depth was less than 0.5 μm for all conditions, which was comparable to the surface roughness. Reliable depth measurements were possible when a significant hole depth was achieved by using multiple-pulse machining.

Because the ablation conditions were found to be free of excessive melt generation, and the ablated zone diameters were easily definable, the model by Liu can be used to estimate the threshold fluence and irradiance when operating under ns pulses. The differences observed in the micrographs were reflected in the calculated ablation threshold fluence and irradiance values, as plotted in Fig. 4. It can be observed that a reverse behaviour is present, i.e., shorter pulses reduce the fluence threshold, but increase the irradiance threshold. The ablation threshold fluence varied between 2 and 4 J/cm^2, whereas the threshold irradiance ranged from 27 to 140 MW/cm^2 as a function of the pulse duration. The ablation threshold fluence tended to increase linearly as a function of pulse duration. The decrease in threshold irradiance relative to pulse duration was best fit by a power function. In other words, the delivery of high peak power in the initial part of the pulse is sufficiently capable of initiating ablation, whereas any additional energy will not result in a significant increase after a certain point. However, it should be noted that when the pulse duration remains the same, the pulses (except for 12 ns and 30 ns durations) change shape non-symmetrically with decreasing energy. It is also worth noting that the estimated laser spot radius (w_0), based on the non-linear regression technique, was also in close agreement with the theoretical value. In Fig. 4, the values of w_0 estimated when calculating the ablation threshold fluence and irradiance for different pulse durations are also reported. Slight variations of ± 1.5 μm compared to the theoretical value are observed. Instead of imposing such variations manually in the calculation, they are directly included in the calculation of the ablation threshold values based on the method used in this work.

Although fluence and irradiation are conventionally employed as material characteristics in laser ablation, they result in the aggregation of time-dependant processes into a single parameter. Therefore, fluence and irradiation are insufficient to differentiate the ablation behaviour with different pulse durations or shapes. The fluence is a parameter that integrates the time-dependant process into a single value of energy, while irradiance is a punctual parameter that negates the effect of the power profile on time. Neither of the two parameters is capable of representing the change in the pulse shape when either the pulse energy or peak power is decreased, or the pulse duration is changed. Accordingly, a simple approach based on pulse decomposition that takes the effect of form into account and includes the effects of peak power, energy and pulse duration can be developed. The comparisons suggest that the peak power delivered in the initial part of the pulses initiates ablation over a larger region, whereas the energy delivered in the tail of the pulse is capable of enlarging the ablation zone. Therefore, the pulse shape was decomposed into different components, namely, the primary peak, the tail, and the added energy in the tail (ΔE). The

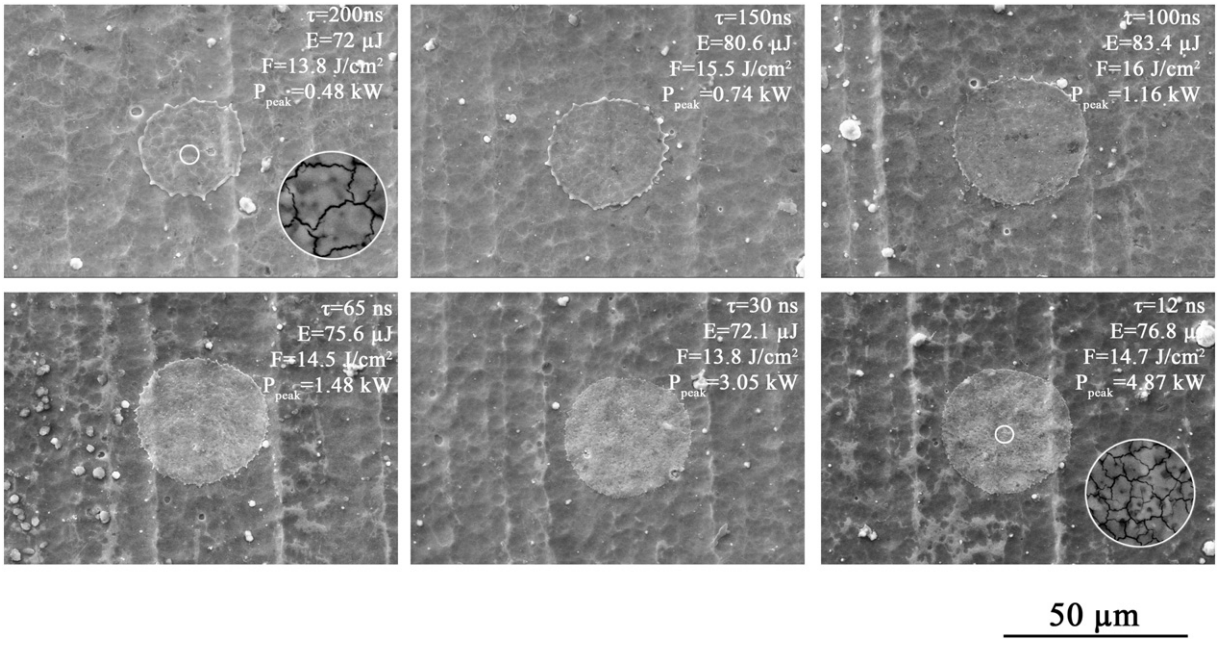

Fig. 2. The evolution of ablated zones with similar energy (E_p) levels and different pulse durations. The small circles in the ablated regions with pulse durations of 200 ns and 12 ns are reported in higher magnification insets to show the crack dimensions. The diameter of the magnified region is 7.7 μm.

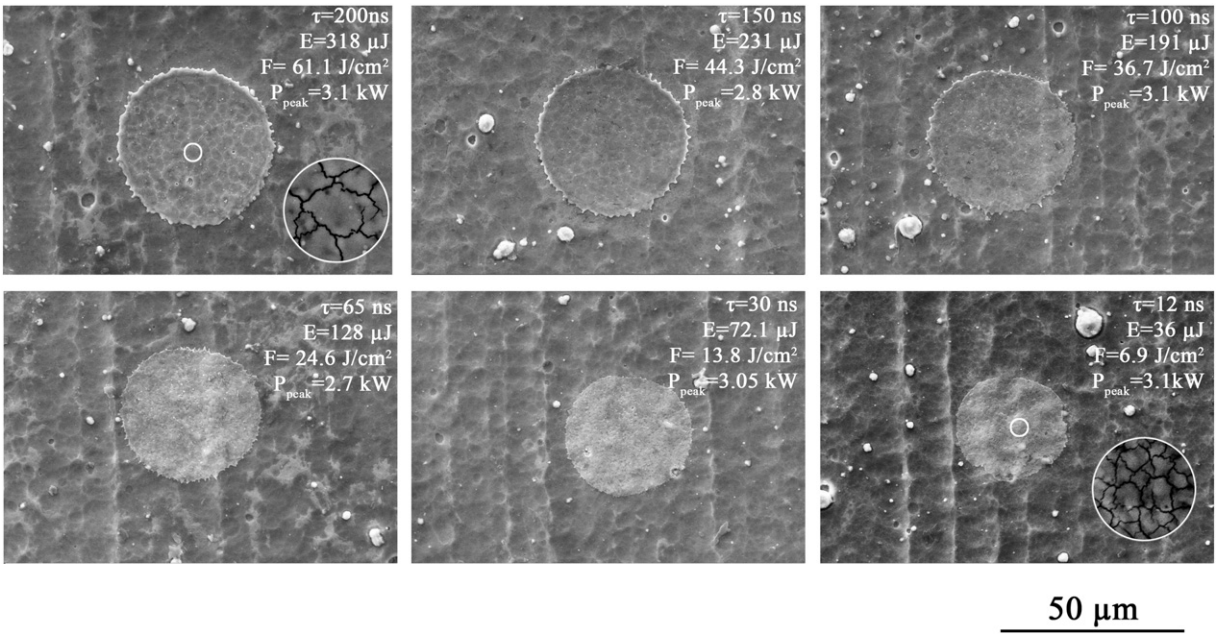

Fig. 3. The evolution of ablated zones with similar peak power (P_{peak}) levels and different pulse durations. The small circles in the ablated regions with pulse durations of 200 ns and 12 ns are reported in higher magnification insets to show the crack dimensions. The diameter of the magnified region is 7.7 μm.

analysis was based on comparing the conditions with the same peak power and different pulse shapes, yielding different pulse energies and durations. Such conditions were identified in the previously measured conditions for peak powers at 2.3 kW, 3.1 kW and 4.1 kW. The data points were extracted in these groups, and their energy contents were compared to the energy content of the shortest pulse of the group. Because the shortest pulses were always 12 ns in duration, the comparison was consistent. Moreover, the 12 ns pulses are symmetric around the peak, which is similar to the fast ascending peak of the other pulse shapes with longer duration. Therefore, it was feasible to decompose each pulse into its primary peak and slowly descending tail, where the primary peak was expressed by the shape of the 12 ns pulse (see the inset of Fig. 5). For a fixed peak power condition (j), the energy of the primary peak was expressed by the energy content of the 12-ns pulse with the same peak power $\left(E_{\tau=12\text{ns},P_{peak_j}}\right)$. For a pulse duration higher than 12 ns (i), the amount of added energy in the tail for the fixed peak power condition (j) is defined with the following expression:

$$\Delta E_{\tau_i,P_{peak_j}} = E_{\tau_i,P_{peak_j}} - E_{\tau=12\text{ns},P_{peak_j}} \tag{8}$$

with

$$\tau_i = [12\text{ ns},\ 30\text{ ns},\ 65\text{ ns},\ 100\text{ ns},\ 200\text{ ns}] \tag{9}$$

and

$$P_{peak_j} = [2.3\text{ kW},\ 3.1\text{ kW},\ 4.1\text{ kW}]. \tag{10}$$

To the best of the authors' knowledge, no theoretical model regarding this decomposition exists; as a result, a regression model was sought using the extracted data points. Fig. 5 shows the extracted data points

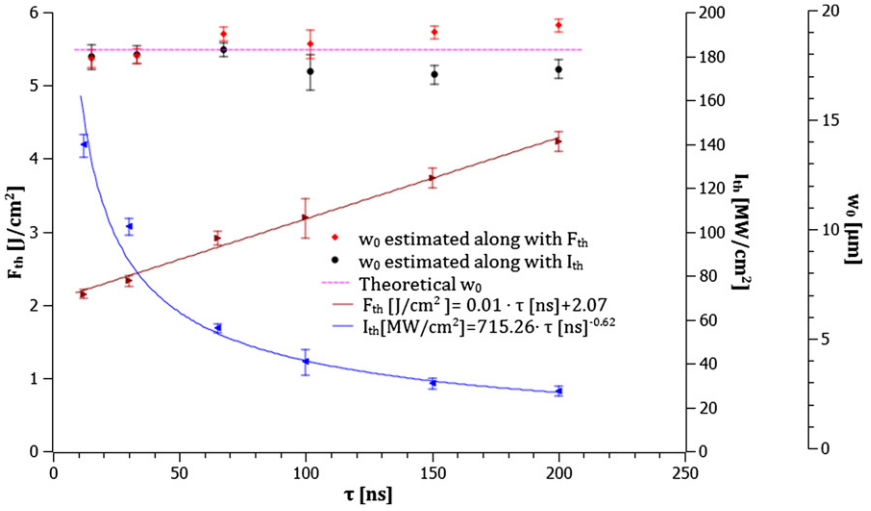

Fig. 4. The results of the single-pulse ablation study: changes in the fluence and irradiance thresholds as functions of pulse duration; the theoretical value of the laser beam radius (w_0); the estimated values for the laser beam based on the non-linear regression method and values of threshold fluence (F_{th}) and irradiance (I_{th}) for different pulse durations. The error bars represent the 95% confidence interval for the mean.

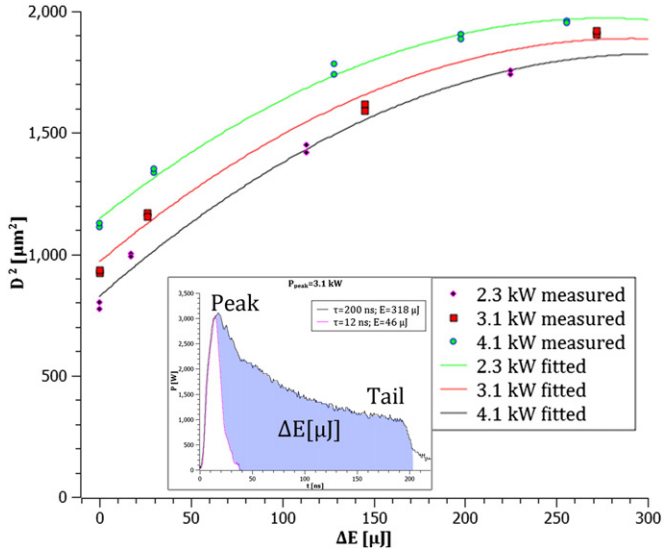

Fig. 5. The effect of the decomposed pulse components on the radius of the ablated area. The inset reports the decomposition of the pulse components, depicting the peak, tail and added energy in the tail (ΔE).

and the fitted regression model for the chosen peak power levels. The extracted data points showed a saturation behaviour as the added energy in the tail (ΔE) increased. The fitted regression model was in agreement with this observation, clearly depicting the saturation in the ablated zone diameter. The fitted model was:

$$D^2\left[\mu m^2\right] = 419.65 + 7.33\Delta E[\mu J] + 177.11P_{peak}[kW] - 0.0108\Delta E^2\left[\mu J^2\right] - 0.3286\,\Delta E[\mu J]P_{peak}[kW]. \quad (11)$$

The model adequately fits the data points, demonstrated by the high values of $R^2_{adj} = 99.05\%$ and $R^2_{pred} = 98.85\%$. The analysis confirms that the ablation process is dependent on the peak power, as well as the pulse energy, and cannot be properly defined by a single term. As the regression model shows, the peak power is more effective in ablating a larger area, whereas the addition of more energy after the initial peak only contributes to a certain level. The tail of the pulse may be useful for increasing the crater depth, but the ablation threshold measures the area of material that effectively interacts with the laser beam. The results show that for precision machining, which requires accurate dimensional control and sustained material integrity, pulse shape should be controlled both in terms of the initial peak power and the tail of the pulse. Moreover, this gives insight regarding how the pulses should be shaped to favour or facilitate ablation, which is crucial for materials with thermal and optical properties that render ablation more difficult.

3.2. Multiple-pulse study

The observations previously made on the extension of the ablated region as a function of the pulse energy and peak power are reflected in the hole depth, as well in the multiple-pulse study. For fixed energy conditions, shorter pulses yielded higher peak powers and resulted in holes with larger diameters. These observations are parallel to those gathered in the single-pulse study. As the number of pulses increased, significant hole depths could be achieved. When ablation conditions yielded hole depths less than or on the order of the coating thickness (approximately 4 µm), the hole profiles were characterised by spherical domes. For longer pules (100 and 200 ns), the edges of the holes showed the significant presence of molten and solidified coating material, which was absent when machining with 12 ns pulses (see Fig. 6). For holes with depths that are significantly higher than the coating thickness, the hole shape depends highly on the machining condition. A spherical shape is maintained for pulses shorter 12 ns, while the geometric integrity decreases with longer pulses (100 ns and 200 ns) due to significant amount of recast substrate layer.

The results suggest that delivering the same amount of energy over a longer pulse duration leads to deeper holes. This can be attributed to the fact that longer pulses have a larger heat penetration depth (d), as expressed in the well-known equation:

$$d = (4\alpha\tau)^{1/2} \quad (12)$$

where α is the thermal diffusivity [16]. The heat penetration depth on TiN is 0.5 µm, 1.5 µm, and 2 µm for pulse durations of 12 ns, 100 ns, and 200 ns, respectively. As the heat penetrates deeper into the material, it is possible to remove larger amounts of material, because the amount of material exposed to temperatures greater than the vaporisation temperature is increased. Consequently, the molten fraction increases, and the process of direct vaporisation from the solid form is accompanied by a removal mechanism that occurs in the form of vaporisation from the molten state. In the case of equal peak powers, longer peak pulses result in deeper and larger holes, as more energy is delivered in the decaying tail of the pulse, which further increases the ablated area size and, consequently, increases the machined depth, as

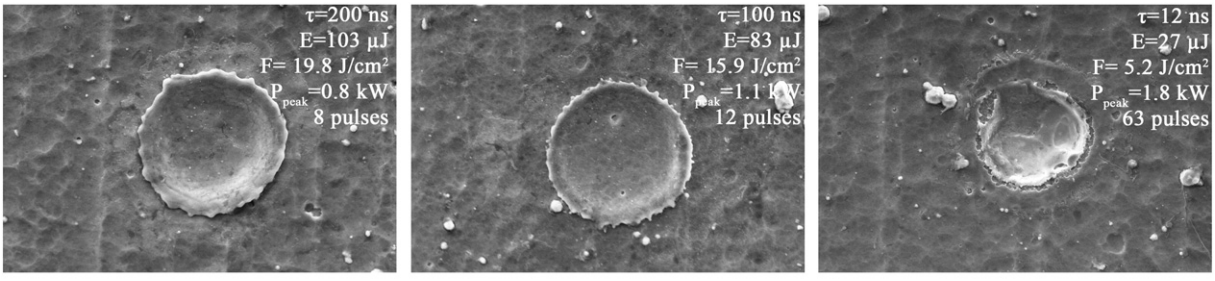

D = 40.2 ± 0.7 µm
h = 5.75 ± 0.34 µm
E_{tot} = 824 µJ
t_{drill} = 400 µs

D = 39.8 ± 0.7 µm
h = 6.3 ± 0.39 µm
E_{tot} = 996 µJ
t_{drill} = 600 µs

D = 36.2 ± 0.2µm
h = 6.7 ± 0.17 µm
E_{tot} = 1701 µJ
t_{drill} = 3150 µs

Fig. 6. A comparison of holes with similar geometric properties obtained with different pulse durations, energy levels and number of pulses.

well. With the shortest pulse duration of 12 ns, no significant machining depth was achievable before 3 pulses. Because these pulses do not possess a decaying tail after the initial peak, no coupling of more energy within the material occurs. This phenomenon is more visible when conditions yielding similar volumes of removed material are compared (see Fig. 6). It can be seen that to remove the same amount of material, pulses of 200 ns in duration are more efficient, because the total amount of energy used is 824 μJ, which is approximately half of the 1701 μJ employed with a 12 ns pulse duration. This suggests that energy transfer changes within the pulse duration. Once energy coupling is achieved and ablation is initiated, which occurs in the initial part of the pulse, the energy within the decaying tail is more effective in material removal. If the same total amount of energy is applied with short pulses, in which a decaying tail is not present, the advantage of energy coupling is not exploited. In contrast, the absence of a decaying tail restricts the material removal mechanism to direct vaporisation, which avoids excessive melt generation and sustains better machining quality.

Fig. 7 depicts the measured diameter and depth values of the drilled holes, as functions of the pulse duration, fluence, and number of pulses. It can be observed that for pulse durations of 100 ns and 200 ns, the number of pulses has little influence on the hole diameter but is highly effective towards increasing the depth, which is a consequence of larger thermal penetration in the material. A decrease in the measured diameters is visible for the two pulse durations with higher numbers of pulses (after the 10th pulse for $\tau = 100$ ns, and the 7th pulse for $\tau = 200$ ns), as a consequence of the deposition of spattered substrate material around the hole entrance. In both cases, this phenomenon is observed as a decrease in the rate at which the drilling depth increases. In comparison to the TiN coating, the substrate material, AISI M2 possesses a similar thermal penetration depth (α) but only half the

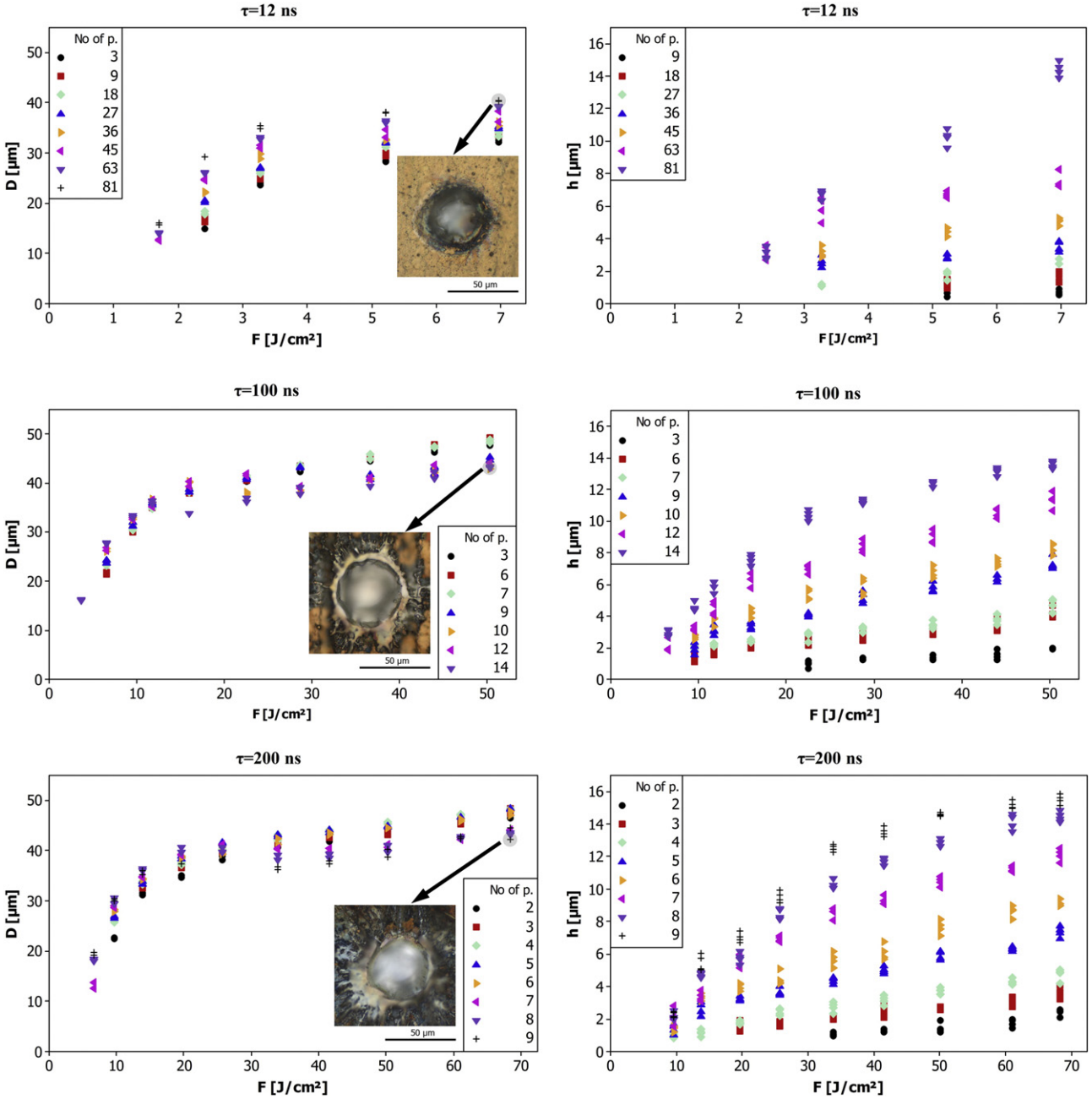

Fig. 7. Hole diameters and depths as functions of the fluence and number of pulses for different pulse durations.

reflectivity at the laser wavelength (R) and half the melting temperature (T_m) (see Table 1). The change in machining behaviour from coating to substrate material serves as a critical point in multiple-pulse ablation. Although not measured directly, a comparison of the physical properties shows that AISI M2 would reach melting and boiling points easier with the applied laser energy. Accordingly, the substrate should possess an ablation threshold that is significantly lower than that of the TiN coating. It should be considered that due to differences in the physical properties of the coating and substrate, the material removal mechanism changes between these layers. Furthermore, higher amounts of molten AISI M2 are expected, due to the lower melting temperature and increased absorptivity of this material. At this point, material removal can be achieved via either direct vaporisation, vaporisation from the molten phase or melt expulsion. The way in which material is removed in the presence of high amounts of the molten phase is critical, because this fact determines the machining quality. Melt ejection can occur due to the recoil pressure of the vaporising material, causing the material to splash in the radial direction. With increasing fluence, the molten material breaks into vapour and droplets as a result of explosive boiling [21]. The fraction of melt generated depends on the pulse length and shape, as well as the fluence and number of pulses. As previously mentioned, the heat penetration depth increases significantly as the pulse duration moves from 12 ns to 200 ns. In the case of 100 ns and 200 ns pulses, the mechanism of material removal from the coating is observed to be direct vaporisation; in contrast, the mechanism for the AISI M2 substrate is melt ejection. The recast layer around the deep holes is characterised by the deposition of large and intact substrate pieces on the coating, rather than the micrometre- and submicrometre-sized droplets observed during explosive boiling (see insets of Fig. 7). During melt ejection, some of the expelled material is re-deposited around the entrance and walls of the hole, causing hole narrowing. Consequently, shadowing effects develop, reducing the amount of laser energy that reaches the bottom of the drilled hole [22]. Moreover, as the hole depth increases, the ejection of molten material becomes more difficult, leading to condensation inside the hole. The build-up of material inside the hole and around its entrance causes a decrease in the ablation rate. With 100 ns and 200 ns pulses, the hole depth increases asymptotically for depths greater than 8 μm. In this size region, the hole depth is significantly larger than the coating thickness, thus the reduction in ablation depth is associated with the melt formation of the steel substrate and the resulting effects. In the case of the 12 ns pulse duration, such a drop in the rate of increase of the diameter or depth of a hole is not visible with increasing pulse number. The pulse duration is sufficiently short that it is able to prevent an excessive quantity of the molten phase from developing on the substrate material. Even when the hole depth is greater than the coating thickness, the ablation process is still dominated by vaporisation, and melt ejection is avoided. This avoids hole narrowing and reduction in the material removal rate. Accordingly, similar material removal rates exist for the substrate and coating materials for the pulse duration of 12 ns. As a result, no asymptotic behaviour is observed for the hole depth.

Another important phenomenon observed with the shorter 12 ns pulse duration is damage accumulation phenomenon. The hole diameter visibly increases when the number of pulses is increased, suggesting the presence of damage accumulation. The phenomenon was first reported by Jee et al. [23], followed by extensive application to the ablation of various materials, including TiN [24–26], using ultrashort ps–fs pulses. The damage accumulation effect is expressed as a reduction in the threshold fluence as:

$$F_{th}(N) = F_{th}(1)N^{S-1} \tag{13}$$

where $F_{th}(N)$ and $F_{th}(1)$ are the ablation threshold fluence of N pulses and a single-pulse, respectively, and S is the incubation coefficient. Lower numbers of S correspond to higher degrees of damage incubation, thus causing the ablation threshold to be lowered. To calculate the ablation thresholds for different numbers of pulses at 12 ns of pulse duration, conditions between 3 and 36 pulses were extracted, because these conditions do not correspond to holes deeper than the thickness of the coating material. Fig. 8 shows the calculated threshold fluences with the fitted model, as expressed in Eq. (13). The experimentally observed decrease in the threshold occurs from $F_{th}(1) = 2.15$ J/cm^2 for a single-pulse to $F_{th}(36) = 1.04$ J/cm^2 for 36 pulses. The calculated incubation coefficient was $S = 0.8 \pm 0.02$. In the literature, the reported incubation coefficient of TiN is $S = 0.87$ with a pulse duration of 130 fs at a pulse repetition rate of 2 Hz and laser wavelength of 800 nm [24]. Compared with the literature, the coefficient calculated in this study depicts higher damage incubation. This can be attributed to the longer pulse duration and higher pulse repetition rate (20 kHz). On metals, the damage accumulation effect has been attributed both to stress–strain energy storage induced on the material during laser ablation and to changes in the surface topography that lead to changes in the absorption characteristics, according to Jee et al. ($\tau = 10$ ns, $\lambda = 1064$ nm PRR = 10 Hz). The damage accumulation observed on the processing of polymeric materials (PMMA) with UV light was attributed to the photo-induced formation of defect centres, which enhanced the absorption of UV light ($\tau = 20$ ns, $\lambda = 248$ nm PRR = 2 Hz) [25]. More recently, damage accumulation during the laser micromachining of ITO semiconductors was attributed to the accumulation of plastic deformation ($\tau =$ 10 ps, $\lambda = 1064$ nm PRR = 200–1000 kHz) [26]. In this study, the damage accumulation observed on TiN fits better with the increase in absorption due to changes in surface topography, as can be observed from the SEM images. Typically observed in fs and ps pulsed machining, the damage accumulation factor also indicates that with 12 ns pulses, the thermal interaction of the beam on the material is limited. The short duration of the pulse allows melt-free machining on the TiN coating, which yields an increase of the hole diameter due to local changes in the optical properties rather than thermal propagation in the radial direction. The damage accumulation effect also has practical implications regarding the productivity of micromachining. Essentially, low energy, short pulses can be used when machining materials with high ablation thresholds. Under such conditions, it is not necessary to increase the pulse duration or energy, thereby avoiding the degrading effects related to melt generation. Productivity can be compensated by increasing the pulse repetition rate, that is, by applying smaller energy packages at higher frequency. However, the limit to the highest applicable pulse repetition rate should also be investigated to avoid heat build-up in the material or the generation of excessive amounts of plasma, which can attenuate the laser beam intensity by scattering or

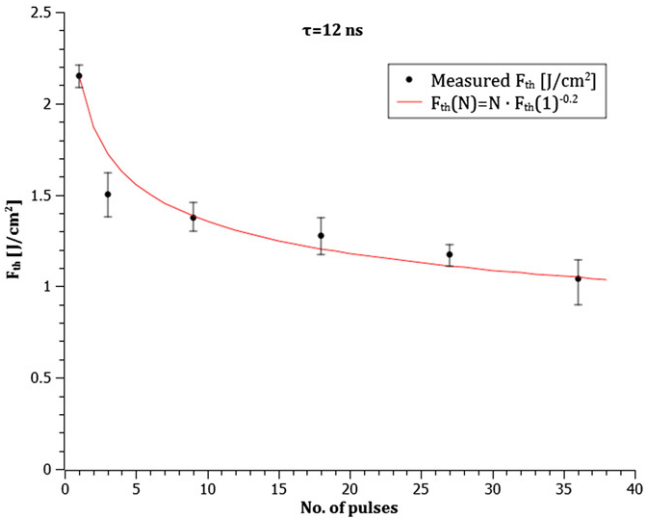

Fig. 8. The fluence threshold as a function of the number of pulses for pulse duration of 12 ns. The error bars represent the 95% confidence interval for the mean.

absorption. The present study did not consider the effect of pulse repetition rate; however, it is expected that the productivity of TiN microdrilling with a pulse duration of 12 ns can be matched to that of 200 ns by increasing the pulse repetition rate to approximately 200 kHz. However, to extrapolate the results to such a degree would require experimental verification, especially to investigate the mentioned degrading effects.

4. Conclusions

Single- and multiple-pulse laser ablation of TiN coatings was studied using a MOPA fibre laser, with programmable pulse shapes and durations between 12 ns and 200 ns. The laser pulses employed in this study were characterised by fast ascending peaks and a decaying tail, which generated a non-symmetric behaviour compared to Gaussian-like pulse shapes. It was experimentally observed that the pulse duration changed the ablation threshold conditions. Shorter pulses required less energy but higher peak power to initiate ablation. Because the pulse shape changed in a non-symmetric manner with the change of pulse energy for a given pulse duration, the pulse shape was decomposed into its initial peak and decaying tail. The decomposition was also expressed mathematically, and a regression model was fitted to the extracted data. The model effectively demonstrated that the energy added in the tail in fixed peak power conditions resulted in the saturation of the ablated region. Although this approach is based on statistical methods, it satisfactorily quantifies the observed phenomenon and the effects of the pulse components, representing a novel attempt to tackle this problem.

In the multiple-pulse study, the effect of pulse duration on hole depth evolution was further investigated. Compared to the shortest pulse duration (12 ns), longer pulses (100 ns, 200 ns) were more efficient in the removal of material from the TiN coating. In comparison, the shortest pulses required higher amounts of total energy to drill the same amount of volume. This effect was attributed to the larger thermal penetration obtained with longer pulses, which caused increased material removal. Drilling beyond the coating thickness while using pulse durations of 100 and 200 ns decreased the hole quality by spattering the substrate material. Due to the lower melting temperature and increased absorption of the laser wavelength, a larger amount of molten layer was generated on the substrate. Thus, the substrate material was ejected in melt form from the realised hole and then condensed around the hole entrance and walls. Such conditions did not occur with 12 ns pulses, due to the confinement of the melt fraction during the process. The number of pulses did not significantly influence the diameter when pulse durations of 100 ns and 200 ns were employed. However, with 12 ns pulses, the number of pulses noticeably influenced the hole diameter. This phenomenon was expressed by the effects of damage accumulation due to changes in material topography, causing higher absorption.

In terms of engineering applications, the results show that there is a larger margin of operation for the micromachining of TiN coatings within the so-called short pulse regime of ns pulses. High-quality machining was demonstrated to be possible, without compromising productivity. Moreover, the fibre lasers presented advantages of robust architecture, simple operation, low capital and operation costs, rendering the applicability of the micromachining of thin surface coatings industrially viable based on this process. In the case of TiN, it was demonstrated that for percussion drilling operations, significant control of hole diameter and depth was achievable. In particular, spatter-free machining conditions were demonstrated, even when drilling beyond the coating into the substrate. For potential laser surface texturing applications, such conditions could be a good solution for increasing the dimple depth without damaging the TiN coating, when machining on substrate materials that are more fragile and strip of easily during operation [27]. Moreover, the addition of pulse duration as a processing parameter extended the operational space. It was possible to realise hole diameters smaller than the laser beam size, as small as 15 μm on one end and up to 50 μm on the other. The hole depth was effectively controlled within the limited thickness of the coating (approximately 4 μm). Such flexibility in terms of hole geometry manipulation should allow the design of patterns and shapes with better precision.

References

[1] H.E. Rebenne, D.G. Bhat, Surf. Coat. Technol. 63 (1994) 1–13.
[2] S. Hogmark, S. Jacobson, M. Larsson, Wear 246 (2000) 20–33.
[3] A. Shenhar, I. Gotman, S. Radin, P. Ducheyne, E.Y. Gutmanas, Surf. Coat. Technol. 126 (2000) 210–218.
[4] H.C. Man, Q. Wang, X. Guo, Opt. Lasers Eng. 48 (2010) 583–588.
[5] A.J. Dowling, M.K. Ghantasala, J.P. Hayes, E.C. Harvey, E.D. Doyle, Smart Mater. Struct. 11 (2002) 715–721.
[6] L. Vandoni, A.G. Demir, B. Previtali, N. Lecis, D. Ugues, Materials 5 (2012) 2360–2382.
[7] S. Marimuthu, A.M. Kamara, D. Whitehead, P. Mativenga, L. Li, Opt. Laser Technol. 42 (2010) 1233–1239.
[8] B.N. Chichkov, C. Momma, S. Nolte, F. von Alvensleben, A. Tunnerman, Appl. Phys. A 63 (1996) 109–115.
[9] B. Gakovic, M. Trtica, T.M. Nenadovic, B.J. Obradovic, Thin Solid Films 343–344 (1999) 269–272.
[10] M.S. Trtica, B.M. Gakovic, L.T. Petkovska, V.F. Tarasenko, A.V. Fedenev, E.I. Lipatov, M.A. Shulepov, Appl. Surf. Sci. 225 (2004) 362–371.
[11] M.S. Trtica, V.F. Tarasenko, B.M. Gakovic, A.V. Fedenev, L.T. Petkovska, B.B. Radak, E.I. Lipatov, M.A. Shulepov, Appl. Surf. Sci. 252 (2005) 474–482.
[12] T.V. Kononenko, S.V. Garnov, S.M. Pimenov, V.I. Konov, V. Romano, B. Borsos, H.P. Weber, Appl. Phys. A 71 (2000) 627–631.
[13] J. Bonse, M. Geuß, S. Baudach, H. Sturm, W. Kautek, Appl. Phys. A 69 (1999) S399–S402 [Suppl.].
[14] W. O'Neill, K. Li, IEEE J. Sel. Top. Quantum Electron. 15 (2) (2009) 462–470.
[15] D.U. Furrer, S.L. Semiatin (Eds.), ASM Handbook, vol. 22A, American Society for Metals, Metals Park, 2009, pp. 599–601, (http://products.asminternational.org/hbk/index.jsp, last access: 19 February 2014).
[16] W.M. Steen, Laser Material Processing, 3rd ed. Springer-Verlag, London, 2003. 79 (198).
[17] H.O. Pierson, Handbook of Refractory Carbides and Nitrides, William Andrew, New Jersey, 1996. 181–208.
[18] A. Schlegel, P. Wachter, J.J. Nickl, H. Lingg, J. Phys. C Solid State Phys. 10 (1977) 4889–4896.
[19] A. Bendavid, P.J. Martin, R.P. Netterfield, T.J. Kinder, Surf. Coat. Technol. 70 (1994) 97–106.
[20] J.M. Liu, Opt. Lett. 7 (5) (1982) 196–198.
[21] N.M. Bulgakova, A.V. Bulgakov, Appl. Phys. A 73 (2001) 199–208.
[22] W. Schulz, U. Eppelt, R. Poprawe, J. Laser Appl. 25 (1) (2013) (012006–1-012006–17).
[23] Y. Jee, M.F. Becker, R.M. Walser, J. Opt. Soc. Am. B 5 (3) (1988) 648–659.
[24] J. Bonse, P. Rudolph, J. Kruger, Baudach, W. Kautek, Appl. Surf. Sci. 154–155 (2000) 659–663.
[25] G.B. Blanchet, P. Cotts, C.R. Fincher Jr., J. Appl. Phys. 88 (5) (2000) 2975–2978.
[26] S. Xiao, E.L. Gurevich, A. Ostendorf, Appl. Phys. A 107 (2012) 333–338.
[27] A.G. Demir, N. Lecis, B. Previtali, D. Ugues, Surf. Eng. 29 (9) (2013) 654–659.